JOURNAL OF SPACECRAFT AND ROCKETS
Vol. 32, No. 2, March–April 1995

# Enhancements to Integral Solutions to Ablation and Charring

Scott A. Leone,* Robert L. Potts,† and Anthony L. Laganelli‡
*Science Applications International Corporation, Fort Washington, Pennsylvania 19034*

**Two new enhancements to the heat-balance integral (HBI) technique improve the rapid prediction of aerothermal response of heat shields of high-speed vehicles. The first enhancement uses a generalized cubic in-depth thermal profile to mitigate the well-known overreaction of classical HBI techniques to rapid changes in aerodynamic heat load. The second enhancement involves a direct method for solving in-depth charring problems in the context of an HBI solution. Together, these enhancements extend approximate HBI techniques to a broader range of aerothermal problems with improved accuracy at only a modest cost in computational speed.**

## Nomenclature

$A$ = profile parameter defined by Eq. (14)
$A_j$ = Arrhenius coefficient (collision frequency), $s^{-1}$
$B_j$ = Arrhenius coefficient (activation temperature), K
$c_p$ = specific heat of ablator, J/(g K)
$c_{pg}$ = specific heat of pyrolysis gas, J/(g K)
$h$ = enthalpy, J/g
$k$ = thermal conductivity of ablator, W/(cm K)
$L$ = thickness of ablative heat shield, cm
$\dot{m}$ = mass flux, g/(cm$^2$ s)
$N$ = number of legs in Arrhenius fit of char reactions
$n$ = profile exponent defined by Eq. (15)
$P$ = boundary-layer pressure, bar
$\dot{q}_{\text{char}}$ = in-depth heat flux absorbed by charring, defined by Eq. (9), W/cm$^2$
$\dot{q}_{\text{cw}}$ = cold-wall heat rate, W/cm$^2$
$\dot{q}_{\text{net}}$ = net heat flux conducted into the surface, W/cm$^2$
$T$ = temperature, K
$t$ = time, s
$s$ = recession, cm
$\dot{s}$ = recession rate, cm/s
$y$ = distance from char front towards surface, cm
$z$ = in-depth distance from moving ablating surface, cm
$z^*$ = $z/\delta$
$\alpha$ = thermal diffusivity of ablator = $k/(\rho c_p)$, cm$^2$/s
$\Delta h_{\text{pyr(g)}}$ = heat of pyrolysis per unit mass of gas produced, J/g
$\delta$ = thermal penetration depth, cm
$\delta_c$ = char depth, cm
$\eta$ = reaction order
$\theta$ = transformed temperature (heat density) defined by Eq. (2), J/cm$^3$
$\rho$ = density, g/cm$^3$

*Subscripts*

$b$ = at the back face
$c$ = of char, or at the char front
$f$ = of formation
$g$ = of pyrolysis gas
$r$ = recovery
$v$ = of virgin
$w$ = at the wall
0 = at $t = 0$

*Superscripts*

$o$ = old (previous) time point
$\tilde{}$ = dummy variable of integration

Presented as Paper 92-0854 at the AIAA 30th Aerospace Sciences Meeting, Reno, NV, Jan. 6–9, 1992; received Jan. 27, 1992; revision received Sept. 30, 1993; accepted for publication Sept. 28, 1994. 

*Staff Scientist; currently consultant, Stoner Associates, Inc., 1200 Walnut Bottom Road, Carlisle, PA 17013. Member AIAA.
†Senior Scientist, 21151 Western Avenue, Torrance, CA 90501. Member AIAA.
‡Chief Scientist, 997 Old Eagle School Road, Suite 215, Wayne, PA 19087. Member AIAA.

## Introduction

FOR over forty years, techniques for the prediction of the aerothermal response of re-entry vehicles have been developed and improved. These techniques have evolved as computer technology has changed. But even with the increased capability of computer speed and storage, the originally popular approximate semi-analytical techniques are still relevant today, especially for mission analyses and optimization studies requiring rapid examination of a large number of cases.

This paper describes how some standard approximate techniques for transient aerothermal prediction have been enhanced to be useful for a more general set of re-entry conditions. In particular, the heat-balance integral (HBI) technique has been extended to treat material response with greater accuracy during protracted periods of laminar and transitional heating and late-time cooldown, thereby handling a wider range of ballistic coefficients and launch as well as re-entry. In addition, this paper describes a direct technique for coupling in-depth charring to HBI, with the result of extending both the accuracy and domain of applicability of HBI.

HBI techniques were developed and promoted particularly by Goodman.[1] Using simple assumed polynomial or exponential shapes for the in-depth thermal profile, the one-dimensional heat conduction equation reduces to a relatively simple formulation that can be coupled with temperature-dependent thermal properties and an ablating surface. The method has been demonstrated for a number of engineering problems, including special enhancements for pulselike and time-varying heat loads,[1,2] realistic surface ablation models,[3–6] and in-depth charring.[3–6] References 4–6 present a more complete survey. Here, we build on this prior work and use techniques suggested by Johns[7] and Kemp[8] in new ways to develop an enhanced HBI featuring a generalized cubic thermal profile and a direct, generalized solution for charring ablation.[9]

## HBI with Generalized Cubic Profile

As shown in a companion paper[6] and in several other sources,[3–5] the one-dimensional heat conduction equation for a noncharring ablator is expressible as

$$\frac{\partial \theta}{\partial t} = \frac{\partial}{\partial z}\left(\alpha \frac{\partial \theta}{\partial z}\right) + \dot{s}\frac{\partial \theta}{\partial z} \tag{1}$$

where

$$\theta = \int_{T_0}^{T} \rho(\tilde{T}) c_p(\tilde{T})\, \mathrm{d}\tilde{T} \tag{2}$$

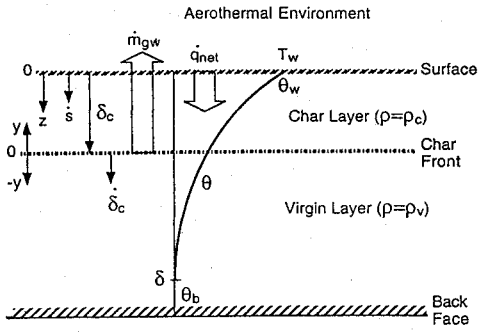


**Fig. 1 Schematic of charring ablator.**

is the transformed temperature (i.e., heat density), $T_0$ is the initial, cool, uniform heat shield temperature, and $\dot{s}$ is the recession rate of the moving (ablating) surface. Figure 1 shows the geometry and notation involved. For a charring ablator, in which the fiber-reinforced plastic thermally decomposes in-depth because of intense surface heating (see again Fig. 1), pyrolysis gas terms must be added to Eq. (1), and auxiliary relations must be set to conserve mass and define the decomposition rate.[5,6,10] Thus, as derived in Refs. 5 and 6,

$$\frac{\partial\theta}{\partial t} = \frac{\partial}{\partial z}\left(\alpha\frac{\partial\theta}{\partial z}\right) + \dot{s}\frac{\partial\theta}{\partial z} + \Delta h_{\text{pyr}(g)}\frac{\partial\dot{m}_g}{\partial z} + \dot{m}_g c_{pg}\frac{\partial T}{\partial z} \tag{3}$$

$$\frac{\partial\dot{m}_g}{\partial z} = \frac{\partial\rho}{\partial t} - \dot{s}\frac{\partial\rho}{\partial z} \tag{4}$$

$$\frac{\partial\dot{m}_g}{\partial z} = -\rho_v\left(\frac{\rho-\rho_c}{\rho_v}\right)^{\eta}\sum_{j=1}^{N} A_j \exp\left(\frac{-B_j}{T}\right) \tag{5}$$

For purposes of developing an HBI solution, certain terms above use the transformed temperature (i.e., heat density $\theta$) while others involve $T$ directly. In order to apply Eq. (2) to a charring ablator, a fixed, monotonic relationship of ablator material density as a function of temperature must be assumed. As shown in Refs. 3–6, actual charring-ablator thermal properties often suggest a unified curve. Use of a single $\rho(T)$ function does not compromise the approximate solution as long as this density function is used only to define Eq. (2) and the in-depth temperature profile and not the in-depth density or effective char depth.[5,6]

To apply the HBI technique, the heat conduction equation must be integrated spatially. Letting $\delta$ represent the effective heat penetration depth, integration of Eq. (3) from 0 to $\delta$ produces

$$\frac{\mathrm{d}}{\mathrm{d}t}\int_0^{\delta}\theta\,\mathrm{d}z - \theta_b\dot{\delta} = \left[\alpha\frac{\partial\theta}{\partial z}\right]_0^{\delta} + \dot{s}\theta\Big|_0^{\delta} + \int_0^{\delta}\left(\Delta h_{\text{pyr}(g)}\frac{\partial\dot{m}_g}{\partial z} + \dot{m}_g c_{pg}\frac{\partial T}{\partial z}\right)\mathrm{d}z \tag{6}$$

where $\dot{\delta}$ denotes the time derivative of $\delta$ and appears on the left side of Eq. (6) according to the Leibnitz rule, and where $\theta_b = \theta(\delta, t)$ denotes $\theta$ at $z = \delta$. The applicable boundary conditions are

at $z = 0$:

$$\frac{\partial\theta}{\partial z} = -\frac{\dot{q}_{\text{net}}}{\alpha_w} \quad \text{and} \quad \theta = \theta_w \tag{7}$$

at $z = \delta$:

$$\frac{\partial\theta}{\partial z} = 0 \quad \text{and} \quad \theta = \theta_b \tag{8}$$

Also, $\dot{m}_g = 0$ for $z > \delta_c$, as discussed later for charring. In the preceding, $\theta_w$ is one of the unknowns to solve for, while $\dot{q}_{\text{net}}$, the net heat flux conducted into the exposed front-face surface, is a known function of $t$ and $\theta_w$, as established by a surface energy balance (see Ref. 4, 5, 6, or 10). This temperature dependence of the net surface heat flux makes the problem interesting, realistic, and difficult. Equation (7) stems from Fourier's law and shows, with Eq. (8), that the first term on the right side of Eq. (6) reduces to $\dot{q}_{\text{net}}$.

To understand the back-face condition, let $L_0$ be the original, initial thickness of the ablator at time $t = 0$. Then transient ablator thickness is $L(t) = L_0 - s(t)$. If $\delta < L$, then $\theta_b = 0$. But if $\delta = L$, then not only is $\theta_b > 0$ possible, it also follows that $\dot{\delta} = \dot{L} = -\dot{s}$, in which case the second term on the left side of Eq. (6) cancels with the upper integrated limit of the second term on the right side of Eq. (6).

To complete integration of Eq. (6), assume a two-layer model for in-depth density in which a moving, infinitesimally thin char front at depth $\delta_c$ divides the outer fully-charred layer from the in-depth virgin layer. Then with $c_{pg}$ also constant, Eq. (6) becomes

$$\frac{\mathrm{d}}{\mathrm{d}t}\int_0^{\delta}\theta\,\mathrm{d}z = \dot{q}_{\text{net}} - \dot{s}\theta_w - \dot{q}_{\text{char}}, \qquad \dot{q}_{\text{char}} = \dot{m}_{gw}[\Delta h_{\text{pyr}(g)} + c_{pg}(T_w - T_c)] \tag{9}$$

as shown in Refs. 5 and 6. Here $\theta_w$, $\delta$, $\dot{m}_{gw}$, and $\delta_c$ are the key unknowns to solve for, and Eq. (2) relates $\theta_w$ and $T_w$. Unlike Ref. 5, though, $T_c$ is not taken as constant in Eq. (9). Instead, a direct solution for $\dot{m}_{gw}$ and $\delta_c$, leading to a transient $T_c$, is presented below.

In order to solve Eq. (9) with HBI, an in-depth thermal profile must be assumed. Two mathematical formulations will be used. The first form is

$$\theta = (\theta_w - \theta_b)(1 - z^*)^n + \theta_b \tag{10}$$

where $z^* = z/\delta$ and the exponent $n$ is variable as defined below. Clearly, a polynomial of this type is applicable only for positive $\dot{q}_{\text{net}}$ in Eq. (7), since the slope $(\partial\theta/\partial z)$ of Eq. (10),

$$\frac{\partial\theta}{\partial z} = \frac{-n(\theta_w - \theta_b)}{\delta}(1 - z^*)^{n-1} \tag{11}$$

is always negative for $0 \le z^* < 1$ and $\theta_w > \theta_b \ge 0$. Therefore, the second in-depth thermal profile function is made more general in shape to accommodate cooldown and a positive slope near the front-face surface. Assuming a general cubic of the form

$$\theta = az^3 + bz^2 + cz + d \tag{12}$$

a positive slope $(\partial\theta/\partial z)$, and thus negative $\dot{q}_{\text{net}}$, becomes possible. Applying the boundary conditions, Eqs. (7) and (8), to Eq. (12) yields

$$\theta = (\theta_w - \theta_b)(1 - z^*)^2(1 - Az^*) + \theta_b \tag{13}$$

where

$$A = \frac{\dot{q}_{\text{net}}\delta}{\alpha_w(\theta_w - \theta_b)} - 2 \tag{14}$$

Equations (13) and (14) show the proper structure of the problem, as not all the coefficients in Eq. (12) are independent of each other; i.e., there are fewer than four degrees of freedom in Eq. (12), despite first glance.

Equations (10) and (13) may both be used during the course of a trajectory. The two equations are identical for $A = 1$ and $n = 3$. Rules for specifying which equation applies at any point of the trajectory and for smoothly transitioning from one equation to the other must be defined. Notice first that at the wall surface ($z^* = 0$), Eq. (7) makes Eq. (11) become

$$n = \frac{\dot{q}_{\text{net}}\delta}{\alpha_w(\theta_w - \theta_b)} \tag{15}$$

Thus, $n = A + 2$. Also notice that in Eq. (13), if $A > 1$, then it is possible for the transformed temperature to be less than zero; namely, $\theta < 0$ for $1/A < z^* < 1$. This negative-heat-density condition is, of course, unrealistic, since it implies values of in-depth temperature that are less than $T_0$ or even negative. Therefore, the limiting condition on Eq. (13) is $A < 1$. If $A \ge 1$, then Eq. (10)

is used. Note that a large $A$ implies a large $\dot{q}_{net}$, which provides a realistic polynomial in-depth profile, since the surface is heating up and thus the slope of the in-depth thermal profile will be negative at the wall. Under cooldown conditions (negative $\dot{q}_{net}$), Eq. (13) must be used, since the slope at the wall may be positive.

To summarize, if $A < 1$, then Eq. (13) is used as the in-depth thermal profile. But if $A \geq 1$, then Eq. (10) is used, where the exponent $n$ is variable. Use of a profile exponent $n$ that is a function of time was first suggested by Johns,[7] but here we specify the time dependence of $n$ in a new way.[9] As discussed under numerical implementation below, $n$ is obtained from $n = A + 2$ using the value of $A$ at the previous time point.

Use of thermal profiles with variable exponent and possible positive slopes near the wall implies an extra degree of freedom in the problem, for which we must find an additional equation. In classical HBI approaches, $n$ is usually fixed, and profiles such as Eq. (13) are not allowed. In that case Eq. (15) is used to relate $\dot{q}_{net}$, $\delta$, and $\theta_w$ so that after integrating the extreme (upper) left side of Eq. (9), a single fundamental HBI equation in one unknown (usually $\theta_w$ but sometimes $\delta$) is produced.[1,3–6] Here, to accommodate the use of variable $n$, variable $A$, and positive slopes during cooldown, we take a different approach. Using physical insight and heuristic reasoning, we assume a time-dependent functional form for $\delta$. This provides the necessary equation to treat the extra degree of freedom and provide closure.

Physically, the thermal conductivities of heat shields of interest are small.[3–6] Moreover, our main goal is to obtain rapid prediction of surface temperature, surface recession rate, pyrolysis gas mass flux through the wall, and char depth. Therefore, heat penetration phenomena deep in-depth have little influence on the surface solution as long as the overall heat is balanced.

Consider the case of a semi-infinite slab ($L = \infty$) in which surface recession and charring are zero, $\dot{q}_{net}$ and $n$ are constant, and Eq. (10) is the assumed profile (with $\theta_b = 0$). In that case Eq. (9) reduces to $\theta_w\delta/(n+1) = \dot{q}_{net}t$. Substitution of Eq. (15) then produces the well-known result $\delta(t) = [n(n+1)\alpha_w t]^{1/2}$. This $\delta(t)$ expression represents the kind of closure equation we are seeking. It may be necessary, however, to compensate for surface recession at least, if not also charring and time-dependent heat loads. Yet merely subtracting time-dependent total recession $s$ from $[n(n+1)\alpha_w t]^{1/2}$ could lead to negative values of $\delta$, so a smooth, always positive transition is required instead.

To treat charring and time-dependent heat loads, we use the observation cited in Refs. 4 and 5 that the char heat absorption flux $\dot{q}_{char}$ is usually proportional to $\dot{q}_{net}$. Therefore, we represent both by a time-averaged value of a proportionally adjusted $\dot{q}_{net}$, which when substituted into Eq. (15) results in a special time-dependent time-averaged value of $\theta_w$, which we denote $\bar{\theta}_1$. Similarly, we represent the time integral of the $\dot{s}\theta_w$ term of Eq. (9) using another time-dependent time-averaged value, $\bar{\theta}_2$. Thus, Eq. (9) becomes

$$\frac{\theta_w\delta}{n+1} = \frac{n\alpha_w\bar{\theta}_1 t}{\delta} - s\bar{\theta}_2 \tag{16}$$

To obtain the smooth, always positive compensation for recession that we desire, we make the heuristic assumption that $\theta_w \approx \bar{\theta}_1 \approx \bar{\theta}_2$. In that case, Eq. (16) reduces to a quadratic equation in $\delta$ whose solution is

$$\delta = \sqrt{n(n+1)\alpha_w t + (n+1)^2 s^2/4} - (n+1)s/2 \tag{17}$$

Note that $\delta > 0$ in Eq. (17) even for large values of $s$. In practice, we have found that a constant value $n = 3$ suffices (corresponding to the point $A = 1$, where our two thermal profile forms are identical), leading to

$$\delta = \sqrt{12\alpha_w t + 4s^2} - 2s \tag{18}$$

Although not rigorous, the justification for Eq. (18) is that "cold" virgin material experiences an in-depth pulse that is not sensitive to wall conditions. Said differently, given an intense heat pulse at the surface, what subsequently goes on at the surface has little effect on the continuing thermal penetration in-depth.

This idea of maintaining the propagation of thermal penetration distance from an initial heat pulse at the surface is similar to the idea behind Goodman's extended method for treating cooldown following a heat pulse.[1] In Goodman's extended method, the solution following the peak heat flux is decomposed into two parts. The first part is based on a thermal penetration distance propagating in accordance with a constant heat flux equal to the peak value. The second part is based on a thermal cooling distance penetrating an otherwise uniformly hot material at the peak temperature in accordance with a negative heat flux equal to the difference between the actual heat flux and the peak heat flux. This second penetration distance accounts for the change in curvature of the in-depth thermal profile during cooldown following a heat flux peak. For temperature-dependent properties, however, our new method seems easier to implement than either Goodman's extended method[1] or Zien's $\theta$-moment method,[2] which may also alleviate the cooldown problem somewhat (see Ref. 6 for further explanation). In any case, we offer a new alternative approach to the cooldown problem.

We must now put the equations in a form suitable for numerical implementation in a computer code. The fundamental equation of the problem is the heat-balance integral of Eq. (9), which we re-express as

$$\int_0^\delta \theta\, dz = \int_0^t (\dot{q}_{net} - \dot{s}\theta_w - \dot{q}_{char})\, d\tilde{t} \tag{19}$$

If $A \geq 1$, then Eq. (10) is used for the thermal profile. The left side of Eq. (19) becomes

$$\int_0^\delta \theta\, dz = \frac{(\theta_w - \theta_b)\delta}{n+1} + \theta_b\delta \tag{20}$$

Using Eq. (15) to replace $\delta$ in Eq. (20), we can express Eq. (19) as

$$\theta_w = \theta_b + \left( \frac{(n+1)\dot{q}_{net}}{n\alpha_w} \int_0^t (\dot{q}_{net} - \dot{s}\theta_w - \dot{q}_{char})\, d\tilde{t} - (n+1)\theta_b(\theta_w - \theta_b) \right)^{\frac{1}{2}} \tag{21}$$

If $A < 1$, then Eq. (13) is used for the thermal profile. The left side of Eq. (19) becomes

$$\int_0^\delta \theta\, dz = \delta\theta_b + \delta(\theta_w - \theta_b)\left(\frac{1}{3} - \frac{A}{12}\right) = \delta\theta_b + \delta(\theta_w - \theta_b)\left(\frac{1}{2} - \frac{\dot{q}_{net}\delta}{12\alpha_w(\theta_w - \theta_b)}\right) \tag{22}$$

where the last step used Eq. (14). Substituting Eq. (22) into Eq. (19) produces

$$\theta_w = \frac{\dot{q}_{net}\delta}{6\alpha_w} + \frac{2}{\delta}\int_0^t (\dot{q}_{net} - \dot{s}\theta_w - \dot{q}_{char})\, d\tilde{t} - \theta_b \tag{23}$$

Numerical implementation of Eqs. (21) and (23) is discussed later.

## Model for In-Depth Charring and Pyrolysis Gas

The specification of the enhanced HBI technique will not be complete until all the parameters in Eq. (9) are defined. In particular, solutions for the variables $\dot{m}_{gw}$, $T_c$, and $\delta_c$ must be obtained. The idea for the new model presented below was suggested by the work of Kemp.[8] Kemp derived a simple solution for the surface recession rate of ablating polymers such as Teflon and epoxy given certain assumptions, such as a thin reaction zone. Here we apply Kemp's technique to the resin of a charring ablator, separate and distinct from the fiber material of the ablator. In effect, the char front is treated as the surface of an ablator of pure resin, independent of the fiber, as if the resin were all that was present in the heat shield.

Figure 1 shows the notation, coordinate systems, and geometry. Note here that $y = \delta_c - z$. The underlying assumptions include the following:

1) A moving char front at depth $z = \delta_c$ (or $y = 0$) divides the outer fully-charred layer ($y \geq 0$) from the in-depth virgin layer ($y < 0$).

2) The resin decomposes completely in a thin zone in the virgin layer just behind (beneath) the char front.

3) The Arrhenius rate law, Eq. (5), applies, where the $B_j$ are large (which contributes to the decomposition zone being thin) and with $\rho$ effectively equal to $\rho_v$.

4) The temperature profile through the decomposition zone is approximately linear.

The second assumption requires further explanation. Let $\xi$ be a small positive number representing the thickness of the resin decomposition zone, and let $\varepsilon$ be an infinitesimally small positive number, $0 < \varepsilon < \xi$. Then charring (resin decomposition) is assumed to take place between $\delta_c + \varepsilon < z < \delta_c + \xi$, or equivalently $-\varepsilon > y > -\xi$. This char "zone" model differs from the char "front" model in Refs. 5 and 6, in which charring takes place between $\delta_c - \varepsilon < z < \delta_c + \varepsilon$, or equivalently $\varepsilon > y > -\varepsilon$. Kemp refers to this difference between a decomposition zone model and a decomposition front model as the difference between a bulk reaction and a surface reaction.[8] In either case, $\xi$ and $\varepsilon$ are made to approach zero, but different energy equations will result, depending upon whether the reactions are "surface" or "bulk."

It now follows from the second assumption that the pyrolysis-gas flux and solid material density are constant in the char layer. Furthermore, in almost all of the virgin layer, the pyrolysis-gas flux is zero and the virgin density is effectively constant. More precisely, $\dot{m}_g = \dot{m}_{gw}$ and $\rho = \rho_c$ (a positive constant) for $0 \leq z \leq \delta_c + \varepsilon$ (or $y \geq -\varepsilon$), and $\dot{m}_g = 0$ and $\rho = \rho_v$ (a constant, $\rho_v > \rho_c$) for $z > \delta_c + \xi$ (or $y < -\xi$).

Continuing to follow Kemp's[8] work, consider a control volume of fixed $y$ thickness and unit area normal to $y$, moving with the char front, and extending from $y = -\varepsilon$ to a large negative $y$ where the solid resin is cool, say $y = -\Lambda$, where $\Lambda$ is a large positive number (effectively, $y = -\infty$). A mass flux of cool solid resin (CSR) enters the control volume at $y = -\Lambda$ because the control volume is moving with the char front. We neglect the fiber for the moment. At the hot end of the control volume ($y = -\varepsilon$, or $y = 0-$), the only mass flux consists of exiting pyrolysis gases, again neglecting the fiber. For this control volume, conservation of mass shows $\dot{m}_{gw} = \dot{m}_{\text{CSR}}$, and conservation of energy becomes,

$$k\frac{\partial T}{\partial y}\bigg|_{y=0-} = \dot{m}_{gw}h_{gc} - (\dot{m}h)_{\text{CSR}} = \dot{m}_{gw}h_{gc} \qquad (24)$$

$$h_{gc} = h_{fg} + \int_{T_0}^{T_c} c_{pg}\,\mathrm{d}T$$

where the enthalpy of the CSR is taken as zero at the initial reference temperature $T_0$, and the temperature at the hot end of the control volume is $T_c$. For materials of interest, the heat of formation of pyrolysis gas, $h_{fg}$, is typically a large positive constant. For the illustrative calculations below, we use the $h_g - h_s$ value from Ref. 10 for both $h_{gc}$ and $\Delta h_{\text{pyr}(g)}$.

At the char front, the local temperature is $T_c$, and beneath the char front, the local temperature varies linearly. Thus

$$T(y) = T_c(1 + Dy) \approx \frac{T_c}{1 - Dy} \qquad (25)$$

for $|Dy| < 1$, where substitution into Eq. (24) reveals $D = \dot{m}_{gw}h_{gc}/(kT_c)$.

Putting the right side of Eq. (25) into Eq. (5) with $\rho = \rho_v$ results in

$$\frac{\partial \dot{m}_g}{\partial z} = -\rho_v\left(\frac{\rho_v - \rho_c}{\rho_v}\right)^{\eta}\sum_{j=1}^{N} A_j \exp\left(\frac{-B_j(1 - Dy)}{T_c}\right) \qquad (26)$$

The assumption of a thin charring reaction zone provides the justification for using $\rho = \rho_v$. Noting now that $y = \delta_c - z$ and $\partial \dot{m}_g/\partial z = -\partial \dot{m}_g/\partial y$, integration of Eq. (26) spatially over $y < 0$ (in effect from $y = -\infty$ to 0) produces

$$\dot{m}_{gw} = \rho_v\left(\frac{\rho_v - \rho_c}{\rho_v}\right)^{\eta}\sum_{j=1}^{N}\frac{A_jT_c}{B_jD}\exp\left(\frac{-B_j}{T_c}\right) \qquad (27)$$

Substituting the expression for $D$ into Eq. (27) and solving for $\dot{m}_{gw}$ produces

$$\dot{m}_{gw} = T_c\left[\rho_v\left(\frac{\rho_v - \rho_c}{\rho_v}\right)^{\eta}\frac{k}{h_{gc}}\sum_{j=1}^{N}\frac{A_j}{B_j}\exp\left(\frac{-B_j}{T_c}\right)\right]^{\frac{1}{2}} \qquad (28)$$

Considering now both fiber and resin, spatial integration of Eq. (4) produces

$$\dot{m}_{gw} = (\dot{\delta}_c + \dot{s})(\rho_v - \rho_c) \qquad (29)$$

for conservation of mass, as derived in Refs. 4–6. The procedure for solving for in-depth charring is now as follows. Use Eq. (29) and values from the previous time point (superscript $o$) to update the location of the char front; i.e.,

$$\delta_c = \delta_c^o + \int_{t^o}^{t}\dot{\delta}_c\,\mathrm{d}\tilde{t}, \qquad \dot{\delta}_c = \frac{\dot{m}_{gw}^o}{\rho_v - \rho_c} - \dot{s}^o \qquad (30)$$

Then, using the updated $\delta_c$, locate the point $z = \delta_c$ in the thermal profile acquired at the previous time point [Eqs. (10) and (13)]. This defines the new $T_c$. Substitution of this $T_c$ into Eq. (28) produces the new $\dot{m}_{gw}$ at the current time point.

The above procedure has two advantages over prior HBI approaches. First, the Arrhenius coefficients $A_j$, $B_j$, and $\eta$ are used directly. Second, the char temperature varies in time. By comparison, consider the hybrid integral–quasisteady solution of Potts.[5,6] In that approach, the user must define a constant effective char temperature beforehand, using, for example, the techniques described in Ref. 6 or Appendix C of Ref. 5. Then $\dot{m}_{gw}$ is obtained by temporarily setting the left side of Eq. (9) to 0 as in a quasi-steady-state (QSS) approach, and also substituting in Eq. (29) with $\dot{\delta}_c = 0$ as in QSS to eliminate $\dot{s}$. The result is

$$\dot{m}_{gw,\text{QSS}} = \frac{\dot{q}_{\text{net}}}{\theta_w/(\rho_v - \rho_c) + \Delta h_{\text{pyr}(g)} + c_{pg}(T_w - T_c)} \qquad (31)$$

The elimination of $\dot{s}$ makes Eq. (31) produce reasonable gas fluxes even when the material undergoes nonquasisteady response. The full HBI of Eq. (9) with the nonzero left side restored is then solved, using Eq. (31) to define $\dot{m}_{gw}$. The char depth is defined essentially by locating the point in the thermal profile where $T = T_c$. Special provisions are added to prevent decharring as the material cools down. References 5 and 6 provide further details.

## Numerical Implementation

In the present method, the fundamental HBI equations to solve are Eq. (21) for $A \geq 1$ and Eq. (23) for $A < 1$. The time integrals are evaluated by the trapezoidal rule with time step $\Delta t$. Note, then, that at a given time point, Eqs. (21) and (23) are essentially nonlinear equations in one unknown, $\theta_w$, for the other variables are essentially known functions of $\theta_w$. At each time point Eqs. (21) and (23) are solved iteratively using the method of bisection. Bisection is guaranteed to converge provided the solution for the current $\theta_w$ can be bracketed. Thus, it does not matter that $\theta_w$ appears on both sides of Eqs. (21) and (23).

Most quantities that depend physically, directly, and instantaneously on surface temperature are solved implicitly within the iterative bisection loop. Other quantities that have a somewhat delayed reaction physically to surface temperature, such as those relating to in-depth charring or the back face, are solved explicitly; i.e., they are updated only once every time step. Certain exceptions are noted below.

Assume a numerical solution has been obtained through an "old" (previous) time $t^o$. The "new" (current) time is $t = t^o + \Delta t$. Upon

marching to the new time point, the char depth is updated first according to Eq. (30). This char depth is applied to the profile from the old time $t^o$ to obtain $T_c$, as described below Eq. (30). Then this $T_c$ is employed in Eq. (28) to define $\dot{m}_{gw}$. Finally, this $\dot{m}_{gw}$ and $T_c$ are used with $T_w^o$ to define $\dot{q}_{\text{char}}$ as in Eq. (9).

The profile exponent $n$ is defined by $n = A^o + 2$, so it is updated only once per time step. Within the iterative bisection loop, values for $\alpha_w$, $\dot{q}_{\text{net}}$, $\dot{s}$, $\delta$, and finally $A$ are calculated using the $\theta_w$ iterate. The $\delta$ calculation uses $s^o$ and is always done using Eq. (18), unless $\theta_b > 0$, in which case $\delta = L$. Such a $\delta$ may not be consistent with the $n$ of Eq. (15) [as used to derive Eq. (21)], since $n$ is updated only once per time step. This explains why the time dependence of $n$ in the present method differs from that in Johns.[7] Nonetheless, the present method produces excellent numerical results, as shown below.

Within the iterative bisection loop, $A$ is calculated via Eq. (14) using the $\delta$ from Eq. (18). Given this $A$, Eq. (21) or (23) is selected to calculate a $\theta_w$ to compare to the $\theta_w$ iterate. Upon convergence, total recession and back-face temperature are updated. Also, $n = A + 2$ may also be applied either here or at the beginning of the solution at the next time point.

To update back-face temperature, one could employ an integral approach. For example, if $A < 1$, the updated total recession leads to an updated $\delta = L$, which leads to an updated $\theta_b$ via Eq. (23). Likewise, Eqs. (19) and (20) lead to an updated $\theta_b$ for $A \geq 1$. However, a one-dimensional finite-difference in-depth conduction model seems to work best. Essentially, the present HBI method provides a fast, accurate solution for $\theta_w$, which becomes the driving front-face boundary condition (source term) for the simple finite-difference back-face solution. In addition, the HBI solution for $\dot{q}_{\text{char}}$ can be applied as a volumetric sink term. Thus, only one relatively simple finite-difference equation is involved. This tandem HBI–finite-difference approach is still much faster on the computer than a fully coupled simultaneous finite-difference solution of Eqs. (3–5).

To start the numerical solution, we assign $n = 3$, as Eqs. (2) and (15) would otherwise imply $n = \infty$. During the first few time steps, $n$ may oscillate, but the oscillations quickly damp out. In the illustrative example below, $n$ jumped from 3 to 6.76 after two initial time steps of 0.05 s each, but then $n$ converged to 4.6 after approximately 2 s.

## Results and Discussion

To illustrate the success of the new method, we use a test case taken from Refs. 4 and 5. The case involves the 40-s flight of a conical re-entry vehicle of small cone half angle (<10 deg) from an altitude of 90 km to 0 km. The heat shield material is a typical charring ablative carbon–resin composite. The aeroheating inputs for a station back on the cone for this test case are given in terms of the cold-wall heat rate $\dot{q}_{\text{cw}}$, recovery enthalpy $h_r$, and boundary-layer pressure $P$ (Table 1). These quantities are combined in a surface energy balance to obtain $\dot{q}_{\text{net}}$, and the latter also depends on the solution for $\theta_w$, or equivalently $T_w$. Functionally, $\dot{q}_{\text{net}} = f(\dot{q}_{\text{cw}}, h_r, P, T_w \text{ or } \theta_w)$.

To keep the example simple, we model the heat shield material surface as an ablating, porous, purely carbon solid through which inert pyrolysis gases inject into the boundary layer but do not themselves react with the boundary-layer gases or solid carbon. The details of this simplified energy balance are presented in Refs. 4 and 6. For a reacting-pyrolysis-gas model, see Ref. 5.

**Table 1 Aeroheating environment for frustum-cone re-entry simulation**

| $t$, s | Flow [a] | $\dot{q}_{\text{cw}}/\dot{q}_{\text{cw,ref}}$ [b] | $h_r/h_{r,\text{ref}}$ [c] | $P/P_{\text{ref}}$ [d] |
|---|---|---|---|---|
| 0 | L | 1 | 9.0 | $10^{-4}$ |
| 10 | L | 15 | 9.0 | $10^{-3}$ |
| 15 | L | 30 | 9.0 | 0.01 |
| 20 | L | 60 | 9.0 | 0.05 |
| 22 | L | 100 | 9.0 | 0.15 |
| 23 | T | 500 | 9.0 | 0.2 |
| 25 | T | 1000 | 9.0 | 0.5 |
| 30 | T | 2500 | 6.0 | 2.0 |
| 35 | T | 500 | 2.0 | 2.5 |
| 40 | T | 20 | 0.5 | 1.5 |

[a] L = laminar, T = turbulent.
[b] $\dot{q}_{\text{cw,ref}} = 1.136$ W/cm$^2$ = 1.0 Btu/(ft$^2$ s).
[c] $h_{r,\text{ref}} = 2326$ J/g = 1000 Btu/lbm.
[d] $P_{\text{ref}} = 1.01325$ bar = 101,325 N/m$^2$ = 1 atm.

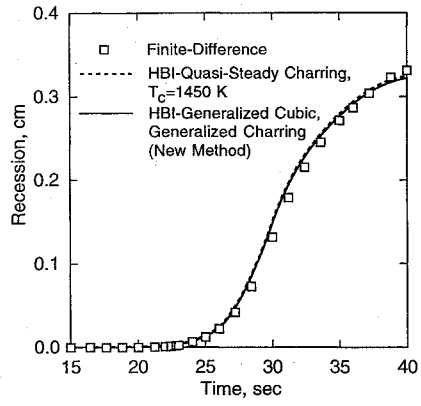


**Fig. 2 Comparison of predictions of surface recession.**

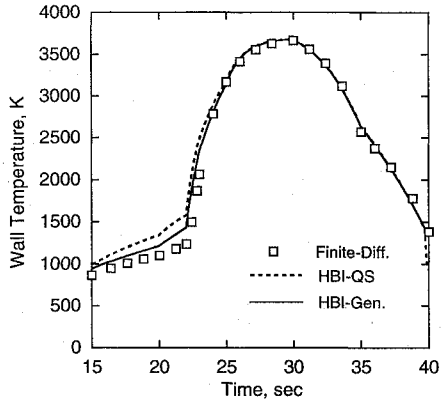


**Fig. 3 Comparison of predictions of wall temperature.**

Also, as shown in Refs. 4–6, the surface energy balance contains a blowing factor of the form $\phi = aB'_0/[\exp(aB'_0) - 1]$, where $B'_0 = \dot{m}h_r/\dot{q}_{\text{cw}}$. In general the blowing parameter $a$ varies with Mach number, flow conditions (laminar or turbulent), and injectant gas species. But again, for simple illustration, we use a constant $a = 1.3$ below, as in Refs. 4–6. (Reference 9 presents a newly updated, alternative form for blowing that may also be of interest.)

The thermal properties used below for the illustrative charring ablator material stem from Table 1 of Ref. 5, or equivalently, Table 2 of Ref. 6. The Arrhenius coefficients we have selected for Eq. (5) are taken from Ref. 10. The pyrolysis-gas specific heat is also taken from Ref. 10.

To show the capability of the new generalized-cubic generalized-charring HBI method, we compare its numerical results with those predicted by a fully coupled finite-difference code developed by Clever and Denny[10] and the HBI–quasisteady charring method of Potts.[5,6] The latter method is represented by Eqs. (9) and (31). The finite-difference solution is considered the baseline that the approximate HBI methods attempt to match.

Figure 2 shows that all three methods produce nearly identical histories of surface recession. Figure 3 shows that HBI methods also approximate the baseline finite-difference temperature history rather well. Note, however, that the temperature history of the new generalized-cubic generalized-charring HBI method approaches the baseline finite-difference history more closely in the preturbulent period (15 to 23 s or so) and late-time cooldown period (39–40 s) than does the HBI method with quasisteady charring. In fact, the final wall temperatures at 40 s are 1384, 938, and 1324 K for the finite-difference, integral–quasisteady, and new generalized HBI approaches, respectively. For longer trajectories (lower ballistic coefficient) such differences are even more pronounced. This shows the special benefit of the new generalized HBI.

Figures 4, 5, and 6 show general agreement of the histories of net heat flux, pyrolysis-gas wall flux, and char depth for both HBI

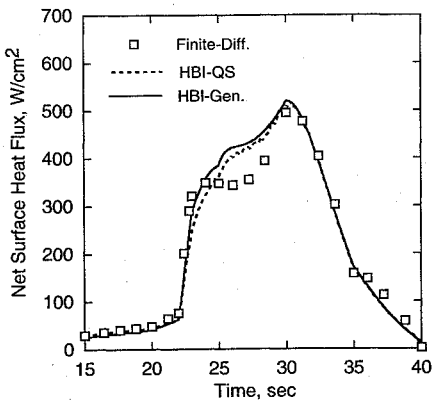


Fig. 4 Comparison of predictions of net surface heat flux.

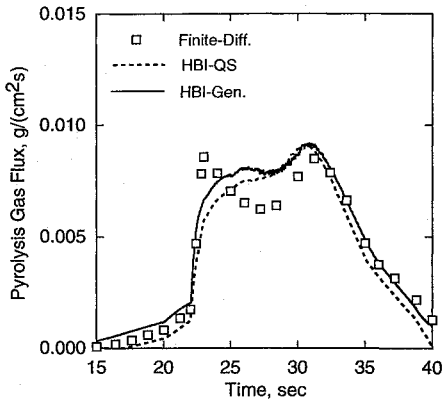


Fig. 5 Comparison of predictions of pyrolysis-gas mass flux at the wall.

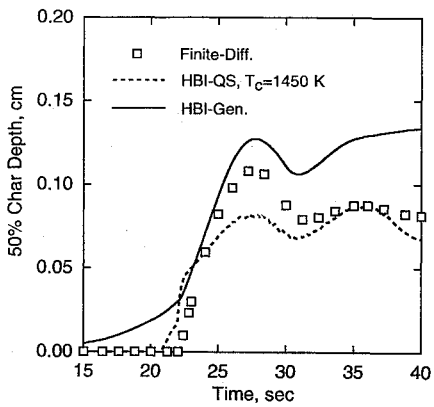


Fig. 6 Comparison of predictions of 50% char depth (measured from the ablating surface).

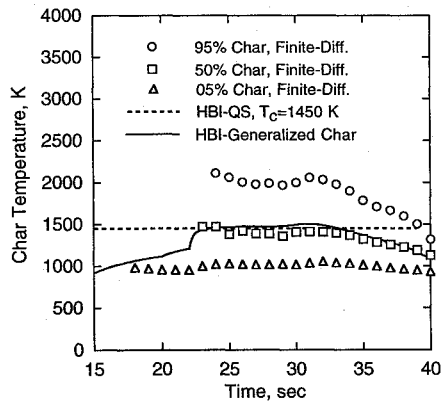


Fig. 7 Comparison of char-temperature calculations and assumptions.

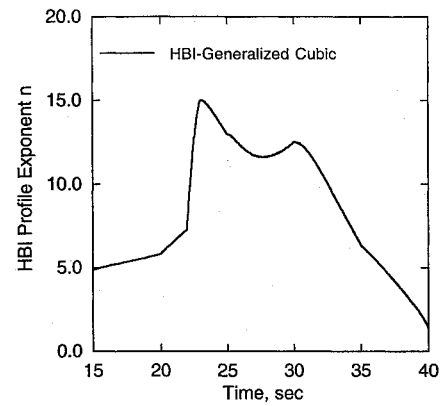


Fig. 8 Calculated history of generalized-cubic-profile exponent.

methods with the finite-difference baseline. For char-depth calculations, the integral–quasisteady method requires the assumption of a fixed effective char temperature. For the clear-air calculations presented here, this effective char temperature was taken as 1450 K after Potts.[4–6] Figure 7 displays clear-air char temperatures predicted (or assumed) by the various methods. As seen, a constant effective char temperature is not a bad assumption, but it is usually more reassuring to let the code calculate a dynamic char temperature (either by the new generalized HBI or by finite difference) rather than having to develop an assumed char temperature beforehand.

Finally, Fig. 8 displays the history of the thermal profile exponent for the new HBI method. After a brief period of oscillation (not shown) due to the startup problem mentioned earlier, $n$ settles down to a value between 4 and 5. Then, as the heating environment becomes more severe at lower altitudes (longer time), $n$ increases. At about 22 s the flow transitions from laminar to turbulent, and $n$ shoots up. This first peak in $n$ reflects the sudden wall heat-flux increase at transition. Then $n$ decreases until the second peak at about 30 s occurs. At 30 s the carbon in this carbon–resin heat shield is ablating at its maximum rate, and the ensuing combustion with air produces an increase in $\dot{q}_{net}$, and thus $n$ increases.

The calculations presented here were performed on a VAX 6440 computer. Run times are primarily a function of the number of time steps and secondarily the convergence criteria and calculational complexity at each time step. In order to prevent oscillations in the charring parameters, the new HBI method requires time steps of about 0.05 s or less and a temperature convergence criterion of about 0.5 K, at least for the sample problem of Table 1 (larger time steps may be satisfactory for problems with less severe transients). The older HBI with quasisteady charring uses a convergence criterion of 5 K and can tolerate time steps of 0.25 s, except during periods of laminar-to-turbulent transition and particle-impact erosion, when 0.05-s time steps are used for accuracy's sake.[4] The finite-difference method used here[10] optimizes time steps dynamically, and these are on the order of 0.02 s for clear-air re-entry.

For the clear-air case of Table 1, run times were 4 CPU seconds for the hybrid HBI–quasisteady charring method, 15 CPU seconds for the new generalized-cubic, generalized-char HBI method, and 50 CPU seconds for the fully coupled finite-difference method. The advantages of the HBI methods for mission analyses, optimization studies, and large parametric investigations are thus obvious.

## Conclusions

Two new enhancements to the HBI method have been presented. First, a generalized cubic thermal profile and a generalized profile exponent produce improvements in accuracy during periods of rapid heatup and later cooldown after peak heating. Second, a generalized model for charring solves the charring equations directly rather than requiring prior development of an effective char temperature. The new HBI method provides more accurate predictions of ablative heat shield response with only a modest cost in computational speed. And the new method is still much faster than fully

coupled finite-difference solutions. This makes it attractive for mission analyses and optimization studies.

## References

[1]Goodman, T. R., "Application of Integral Methods to Transient Nonlinear Heat Transfer," *Advances in Heat Transfer*, Vol. I, edited by T. F. Irvine and J. P. Hartnett, Academic Press, New York, 1964, pp. 51–122.

[2]Zien, T. F., "Integral Solutions of Ablation Problems with Time-Dependent Heat Flux," *AIAA Journal*, Vol. 16, No. 12, 1978, pp. 1287–1295.

[3]Laganelli, A. L., Harper, T. P., and Fogaroli, R. P., "Integral Solution for Thermal Performance of a Charring Ablator," *Heat Transfer with Thermal Control Applications*, edited by M. M. Yovanovich, Vol. 39, Progress in Astronautics and Aeronautics, AIAA and MIT Press, Cambridge, MA, 1975, pp. 375–393.

[4]Potts, R. L., "On Heat Balance Integral Solutions of Carbonaceous Ablator Response During Re-entry," AIAA Paper 84-0393, Jan. 1984.

[5]Potts, R. L., "Hybrid Integral/Quasi-Steady Solution of Charring Ablation," AIAA Paper 90-1677, June 1990.

[6]Potts, R. L., "Application of Integral Methods to Ablation Charring Erosion, A Review," *Journal of Spacecraft and Rockets*, Vol. 32, No. 2, 1995, pp. 200–209.

[7]Johns, D. J., "Comments on 'New Methods in Heat Flow Analysis'," *AIAA Journal*, Vol. 4, No. 6, 1966, pp. 1151, 1152.

[8]Kemp, N. H., "Surface Recession Rate of an Ablating Polymer," *AIAA Journal*, Vol. 6, No. 9, 1968, pp. 1790, 1791.

[9]Leone, S. A., and Laganelli, A. L., "Enhancements to Approximate Ablation Techniques," AIAA Paper 92-0854, Jan. 1992.

[10]Clever, R. M., and Denny, V. E., "Response of Charring Ablators to Severe Aerodynamic and Erosion Environments," *Journal of Spacecraft and Rockets*, Vol. 12, No. 9, 1975, pp. 558–564.

T. C. Lin
*Associate Editor*